American Mineralogist, Volume 77, pages 545–557, 1992

Conversion of perovskite to anatase and TiO_2 (B): A TEM study and the use of fundamental building blocks for understanding relationships among the TiO_2 minerals

JILLIAN F. BANFIELD,* DAVID R. VEBLEN
Department of Earth and Planetary Sciences, The Johns Hopkins University, Baltimore, Maryland 21218, U.S.A.

ABSTRACT

TiO_2 crystallizes in at least seven modifications encompassing several major structure types including those of rutile, hollandite, and PbO_2. We have adopted a fundamental building block (FBB) approach in order to understand better the relationships between these structures. The identification of common structural elements provides insights into possible phase transformation mechanisms as well as the weathering reactions that convert perovskite ($CaTiO_3$) to TiO_2 anatase and TiO_2 (B).

We have studied the weathering of perovskite from the Salitre II carbonatite, Minas Gerais, Brazil, by transmission electron microscopy. Although the dissolution of perovskite, a proposed component of the high-level nuclear waste form Synroc, has been modeled thermodynamically and studied experimentally, its direct natural replacement by Ti oxides during weathering has not been previously described. Our results show that the perovskite is replaced topotactically by both anatase and TiO_2 (B). The reaction appears to involve an intermediate product that can be interpreted as a half-decalcified, collapsed derivative of perovskite. The second step, involving removal of the remaining Ca, can occur in one of two ways, leading either to anatase or in rare cases to TiO_2 (B). The orientations of the interfaces between both perovskite and anatase and perovskite and TiO_2 (B) are consistent with collapse of the corner-linked Ti-O framework to form edge-sharing chains. Despite the orthorhombic structure of perovskite, the results show that the anatase can develop with its **c** axis parallel to any of its three pseudocubic axes. The complete destruction of perovskite produces arrays primarily of anatase that display a variety of textures, including porous aggregates and recrystallized needles. REE elements released from perovskite are immobilized by precipitation of rhabdophane that is intimately intergrown with anatase.

INTRODUCTION

There are currently four naturally occurring TiO_2 polymorphs [rutile, anatase, brookite, and TiO_2 (B)] and at least three (plus some very high-pressure forms) polymorphs that have been produced synthetically. Details for six of the distinctive polymorph structures are listed in Table 1. It is generally considered that at low pressures only rutile has a true field of stability; anatase and brookite form metastably (Dachille et al., 1968; Post and Burnham, 1986). Post and Burnham (1986) used ionic modeling to show that the electrostatic energies of rutile, anatase, and brookite are not greatly different. Navrotsky and Kleppa (1967) measured $\Delta H = -5.27$ kJ/mol for the anatase to rutile reaction.

The structure of the most commonly occurring and best known TiO_2 phase, rutile, is shared by a number of minerals including pyrolusite, cassiterite, stishovite, and in a distorted form, marcasite. The $CaCl_2$ polymorph of TiO_2 is related to the rutile structure by a second-order phase transformation (discussed by Hyde, 1987). The high-pressure polymorph, TiO_2 II, has the α-PbO_2 structure; the highly metastable TiO_2 (H) polymorph has the hollandite structure; and TiO_2 (B) has a structure that is closely related to that of VO_2 (B). The similarities between some of these polymorphs and the related structures of anatase and brookite will be discussed below.

All of the polymorphs contain edge- and corner-linked, octahedrally coordinated Ti cations. The available structure refinements (see asterisks in Table 1) show relatively constant Ti-O distances and quite variable O-O distances, particularly when the shared vs. unshared octahedral edges are compared. Pairs of face-sharing octahedra (containing trivalent Ti) are found only in crystallographic shear structures in reduced rutile derivatives (TiO_{2-x}).

Previous discussions of the relationships between certain of these structures have focused on the presence of sheets of O atoms that approach a cubic closest-packing arrangement (such as in anatase), very distorted hexagonal closest packing that approaches cubic (as in rutile; Hyde et al., 1974), or an approximately double hexagonal

* Present address: Department of Geology and Geophysics, University of Wisconsin–Madison, 1215 West Dayton Street, Madison, Wisconsin 53706, U.S.A.

0003–004X/92/0506–0545$02.00

TABLE 1. Data for some TiO_2 polymorphs and perovskite

Structure	Space group	Density (g/cm^3)	Unit-cell data (nm)	Reference
Rutile*	$P4_2/mnm$	4.13	$a = 0.459$, $c = 0.296$	Cromer and Herrington (1955)
Anatase*	$I4_1/amd$	3.79	$a = 0.379$, $c = 0.951$	Cromer and Herrington (1955)
Brookite*	$Pbca$	3.99	$a = 0.917$, $b = 0.546$, $c = 0.514$	Baur (1961)
TiO_2 (B)	$C2/m$	3.64	$a = 1.216$, $b = 0.374$, $c = 0.651$, $\beta = 107.29°$	Marchand et al. (1980)
TiO_2 II*	$Pbcn$	4.33	$a = 0.452$, $b = 0.550$, $c = 0.494$	Simons and Dachille (1967)
TiO_2 (H)	$I4/m$	3.46	$a = 1.018$, $c = 0.297$	Latroche et al. (1989)
Perovskite*	$Pcmn$	4.03	$a = 0.537$, $b = 0.764$, $c = 0.544$	Kay and Bailey (1957)

* Structures refined by X-ray diffraction.

closest-packing arrangement (as in brookite). These descriptions emphasize differences among the structures but fail to highlight their close relationships.

Andersson (1969) showed that rutile could convert to the TiO_2 II structure by cation displacement. Simons and Dachille (1970) noted that similar structural elements are present in anatase and TiO_2 II and suggested that a transformation between cubic closest-packed and hexagonal closest-packed arrangements involves shear between O layers.

Bursill and Hyde (1972) and Hyde et al. (1974) described a relationship between hollandite and rutile structures involving rotation of adjacent rutile blocks by clockwise and counterclockwise rotation. Alternatively, Bursill (1979) demonstrated that the hollandite structure can be generated from the rutile structure by intersecting antiphase boundaries or crystallographic shear. Latroche et al. (1989) reported that the TiO_2 (H) polymorph converted to anatase rather than rutile with increasing temperature and noted that the structural relationship between TiO_2 (H) and anatase was not clear.

The dissolution of perovskite and its replacement by TiO_2 has been studied experimentally under a range of hydrothermal conditions (e.g., Myhra et al., 1984; Kastrissios et al., 1986, 1987; Jostsons et al., 1990). The interest is partly due to the proposal that perovskite could be a major component of the synthetic assemblage of titanate minerals known as Synroc, a potential nuclear waste form. Thermodynamic calculations have clearly shown that perovskite is unstable with respect to both titanite and rutile at low temperatures and in natural waters (Nesbitt et al., 1981). Kastrissios et al. (1987) suggested that perovskite dissolved under hydrothermal conditions (between 110 and 190 °C) and that euhedral anatase and brookite crystals grew epitaxially from an amorphous Ti-O layer. Jostsons et al. (1990) summarized much of the experimental work on perovskite dissolution including data of Pham et al. (unpublished data), which suggest that under epithermal conditions (<80 °C) an amorphous Ti-rich layer approximately 10 nm thick forms on the perovskite surface. This layer is believed to incorporate Ca ions and act as a protective barrier that inhibits further dissolution.

The first part of this paper describes the results of our attempts to find a unified way of describing the Ti oxide structures. The approach, based on the use of fundamental building blocks (FBB; Moore, 1986), emphasizes the similarities between the structures. The aim is to provide insights into possible direct mechanisms by which polymorphic phase transformations involving TiO_2 might occur. We discuss the application of this view to understanding the TiO_2 (B)–anatase transformation. In the second part of this paper we use the FBB description as well as experimental results to describe perovskite ($CaTiO_3$)–TiO_2 weathering reactions.

An FBB approach to the structural relationships between rutile, anatase, brookite, TiO_2 (B), and TiO_2 (H)

There are many ways to describe structures and the relationships between them. For example, the utility of the polysomatic-series approach has been discussed in detail by Veblen (1991). Although this structural rationalization works well for many minerals, it cannot be simply applied to describe the TiO_2 polymorphs, primarily because of the absence of slabs common to all polymorphs. As noted in the introduction, both crystallographic shear models and descriptions based upon the geometry of the O framework have been used to describe and relate some of the TiO_2 structures. In this discussion, we take a rather different approach. Following Moore (1986), we describe the TiO_2 structures in terms of their construction from a single structural unit, or FBB, by either direct assembly or shear. This approach reveals both the close relationships (some groups of TiO_2 polymorphs contain common structural layers) and the differences between members of the group (e.g., in the stacking of these layers).

Choice of an FBB

The attempt to use an approach based on the presence of common structural elements in the TiO_2 polymorphs was hampered by two problems. First, the largest structural block common to all of them is merely a pair of edge-sharing octahedra. Second, the group of TiO_2 structures falls into two categories, namely, those that contain chains of edge-sharing octahedra in one orientation [TiO_2 (B), anatase] and those with chains in two orientations [rotation parallel to the chain relates the two orientations, e.g., in rutile, brookite, TiO_2 (H)].

All of these structures except rutile can be constructed from a unit composed of four edge-sharing octahedra.

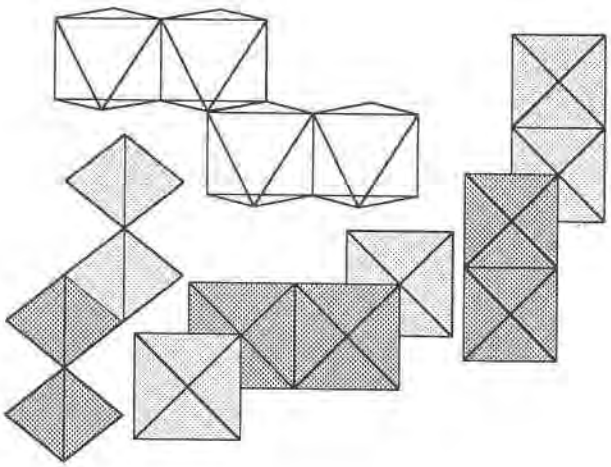

Fig. 1. Representations of the fundamental building block. If light-stippled octahedra have a coordinate $z = 0,1$ (z perpendicular to the page), then dark-stippled octahedra are located at $z = 0.5$.

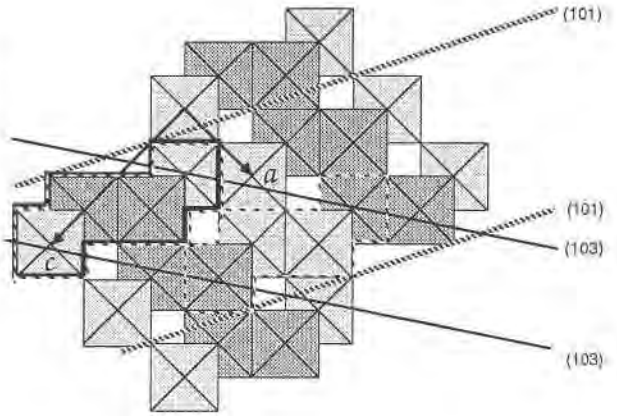

Fig. 2. FBB representation of anatase. The (101)- and (103)-bounded slabs are indicated. The FBB is shown by the solid dark line, and the octahedra included in the (103)-bounded slab are grouped by the dashed line.

Because the basic rutile structural elements can be created by stacking of this unit and the rutile structure itself can be generated from this assembly by shear, we have selected this four-octahedron unit to be the fundamental building block. The FBB is illustrated in four orientations in Figure 1.

Although we will not discuss it further, this FBB also occurs in many structures other than the TiO_2 polymorphs. For example, it is the same as a four-octahedron segment of the M1 cation chain found in the pyroxenes, and it occurs as a fragment of dioctahedral and trioctahedral sheets in the layer silicates, oxides, and hydroxides.

Anatase, brookite, TiO_2 (B), and TiO_2 II and their relationships to rutile

There are a number of reasons to begin this discussion with the anatase structure. Anatase is an important low-temperature alteration product of many Ti-bearing minerals (biotite, pyroxene, perovskite), and a number of thermally induced polymorphic transformations involving this mineral have been reported. The anatase-rutile reaction that occurs during low-grade metamorphism was studied experimentally by Shannon and Pask (1964) and subsequently (with conflicting results) by Kang and Bao (1986). The conversion of both TiO_2 (H) (Latroche et al., 1989) and TiO_2 (B) (Brohan et al., 1982) polymorphs to anatase has been reported. The structural rationalization for the TiO_2 (B) to anatase transformation is well understood (Brohan et al., 1982; Tournoux et al., 1986; Banfield et al., 1991). However, an explanation for the TiO_2 (H) to anatase transformation has not been provided.

A representation of a slice of the anatase structure constructed from the FBB (in the orientation shown on the far right in Fig. 1) is given in Figure 2. Consecutive layers stack directly above the layer shown, linked by corner sharing, so that light-stippled octahedra at $y = 0,1$ define the corners of the unit cell as shown. Dashed parallel lines isolate a (101)-bounded slab of anatase referred to in the discussion of the brookite structure, and those labeled (103) separate groups of octahedra (outlined) that form slabs common to the TiO_2 (B) structure.

Figure 3 shows a representation of a slice through the TiO_2 (B) structure. The FBB is indicated by the heavy solid line, and the corner-linked FBB slab common to the anatase structure (Fig. 2) is shown by the dashed outline. The common structure parallel to (103) anatase rationalizes that TiO_2 (B) is converted to anatase by shear involving growth of ledges along the (103) planes of anatase (Banfield et al., 1991).

The FBB representation of the brookite structure is shown in Figure 4a. This diagram illustrates that brookite

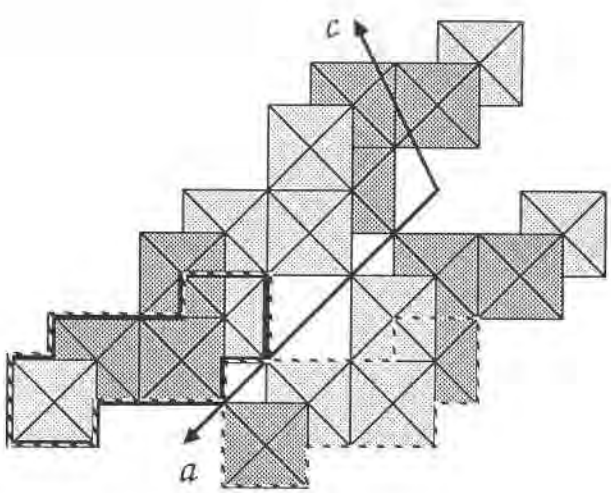

Fig. 3. FBB representation of TiO_2 (B). The FBB is shown by the dark solid line, and the (103)-bounded anatase slab is highlighted by the dashed line.

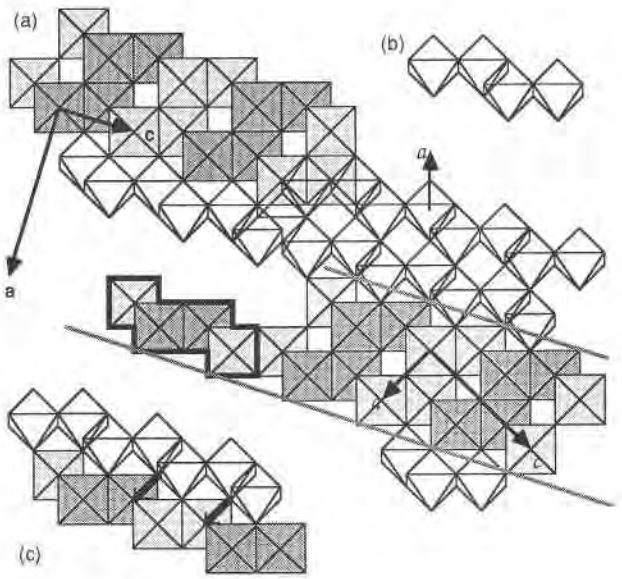

Fig. 4. (**a**) FBB representation of the brookite structure. The dark line shows the FBB, and the dashed line highlights the (101)-bounded anatase slab. Arrows indicate the brookite axes (bold) and the anatase directions (italics) in the plane of the slabs, (**b**) the FBB in the second orientation, (**c**) structural element related to the rutile structure by shear, as indicated by the arrows.

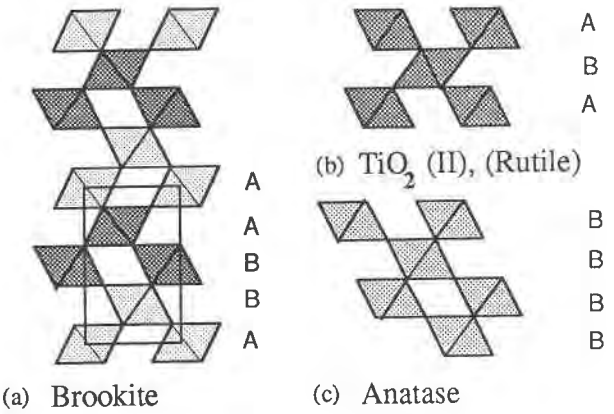

Fig. 6. The stacking of slabs shown in Figures 5a and 5c (A and B) (**a**) to form brookite, (**b**) to form TiO_2 II. The same stacking of slabs containing straight rather than kinked chains produces rutile (**c**) to form anatase.

can be constructed from structural slabs found in anatase (the {101}-bounded slabs). In brookite, these slabs occur in two alternating orientations, shown in Figure 4a as stippled and unstippled. Figure 4b shows the orientation of the FBB for the unstippled slab. The first anatase slab (stippled) is oriented with an anatase **a** axis coming out of the page, the second with an anatase **a** axis vertical.

Figure 4c shows a strip of brookite structure that occurs along the plane where the stippled and unstippled anatase-type slabs are joined. This strip can be converted into the basic unit of the rutile structure (110 rutile slab) by shear, as indicated by the arrows. When viewed down **c** of brookite, shear of this type throughout the structure produces infinite edge-linked chains (out of the page). Alternatively, conversion of these chains to infinite chains could involve cation hopping (every second pair along the chains in Fig. 5 to form straight, edge-sharing horizontal chains) rather than shear. Similar cation displacements relating rutile and TiO_2 II are discussed by Simons and Dachille (1970) and Hyde and Andersson (1988).

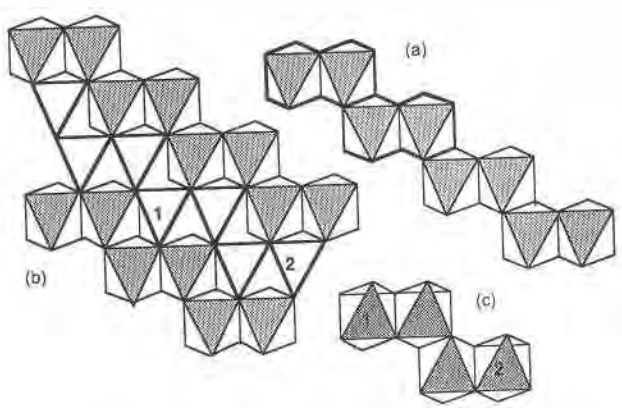

Fig. 5. (**a**) Assembly of an FBB to form a chain, (**b**) arrangement of chains to form sheets found in both anatase and brookite [the (100) plane of brookite], (**c**) an FBB that forms sheets identical to those in **b** but rotated 180°. The numbers indicate how the sheet in **c** may be superimposed onto that in **b**.

Figure 5 shows the arrangement of chains of FBBs (Fig. 5a) that form the (100) layers of brookite, the (101)-bounded slabs of anatase, and the (100) layers of TiO_2 II. The stacking of layers as shown in Figure 5b (A) or identical layers with an orientation as shown Figure 5c (B) generates the structural arrangements illustrated in Figures 6a (brookite: AABBAABB . . .), 6b (TiO_2 II, and by rearrangement as discussed for Fig. 4c, rutile: ABAB . . .), and 6c (anatase: BBB . . .). Thus, ignoring the polyhedral distortions, anatase, brookite, and TiO_2 II can be considered to be simply polytypes of TiO_2 based on stacking of layers illustrated in Figure 5b.

A 180° rotation of octahedra relates the A- and B-type layers suggesting, as noted by Simons and Dachille (1970), that transformations between structures involve shear between O planes. A similar mechanism involving shear of the O planes parallel to the planes of octahedra was postulated for the enstatite to clinoenstatite transformation (Coe and Kirby, 1975). Although such mechanisms involving two sets of shear operations or cation hopping plus shear would convert anatase or brookite to rutile, we currently have no direct evidence to indicate the actual mechanisms by which the transformations occur, and other mechanisms may well operate.

The TiO_2 (H) structure and its relationship to the other polymorphs

An FBB representation of the TiO_2 (H) (hollandite) structure is given in Figure 7. Unlike the structures de-

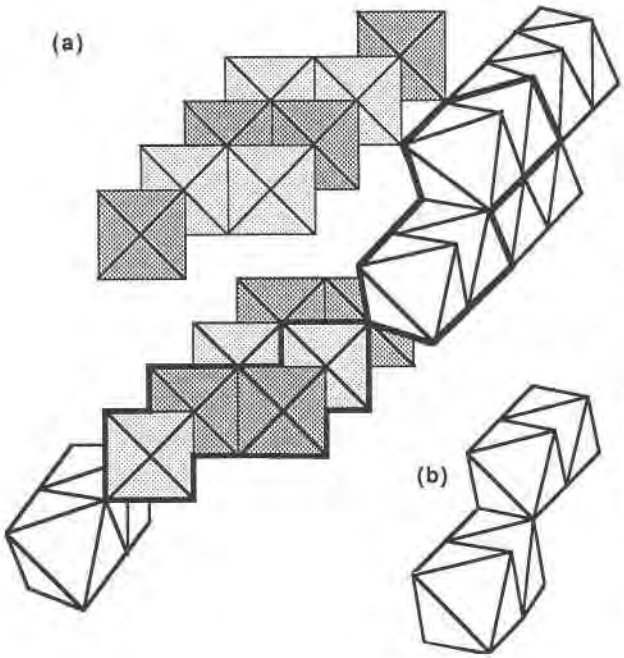

Fig. 7. FBB representation of the basic unit of the TiO_2 (H) structure. The structure contains two orientations of chains constructed from the FBB highlighted by the dark lines (**a**) and in a second orientation (**b**).

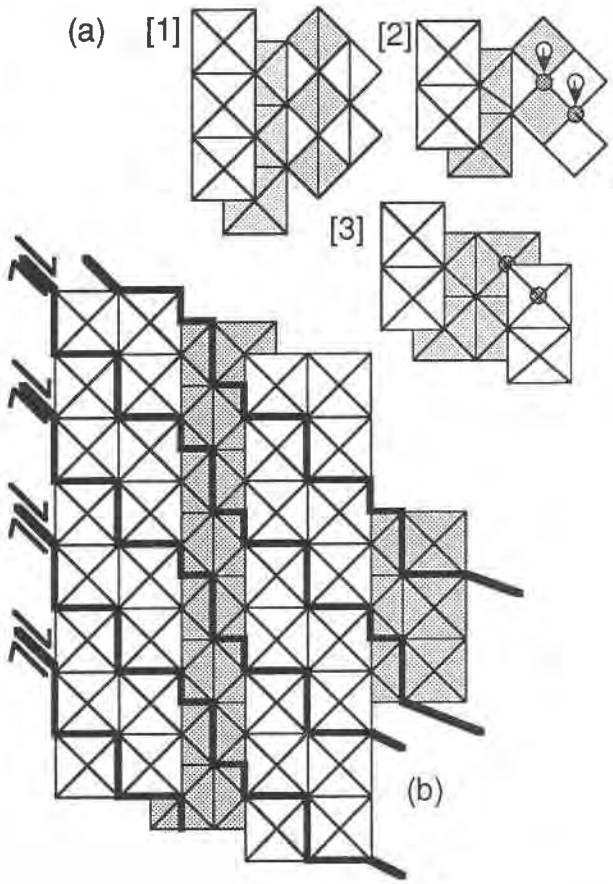

Fig. 8. (**a**) Diagram illustrating the conversion of two chain orientations in TiO_2 (H) to one by cation hopping: [1] = TiO_2 (H) structure, [2] = cation displacement; [3] = resulting structure. (**b**) Arrows indicate the shear needed to transform [3] to TiO_2 (B).

scribed above, in TiO_2 (H) the FBBs are stacked to form infinite chains of edge-linked octahedra; these chains occur in two orientations. The TiO_2 (H) polymorph seems structurally more closely related to rutile than to anatase, and it has been shown that electron-beam damage can result in the conversion of synthetic hollandite compounds to the rutile structure (Bursill, 1979). Consequently, it is interesting that Latroche et al. (1989) report the conversion of TiO_2 (H) to anatase with increasing temperature. A possible mechanism for this reaction involves displacement of cations from the chains in one orientation into adjacent octahedral sites (Fig. 8a), followed by shear as indicated in Figure 8b. This produces the TiO_2 (B) structure, which can in turn be converted to anatase by the previously reported shear mechanism. If this type of structural transformation occurs, we predict that TiO_2 (B) develops as an intermediate phase between TiO_2 (H) and anatase.

The structural relationships between perovskite and TiO_2 structures

It has been previously noted that the TiO_2 (B) structure can be described as a derivative of the ReO_3 structure (Tournoux et al., 1986). Likewise, the perovskite structure is closely related to the ReO_3 structure (Hyde and O'Keefe, 1973). In perovskite, Ca sits within a corner-linked Ti-O framework that is identical to that found in ReO_3 (i.e., perovskite is a stuffed derivative of ReO_3). Consequently, there are close similarities between the perovskite and TiO_2 (B) structures. The relationships noted in the preceding section thus imply that anatase, brookite, TiO_2 II, and in a more complex way, rutile are also related to the perovskite structure.

Experimental methods and samples used

We studied naturally weathered perovskite crystals from the Salitre II carbonatites in Minas Gerais, Brazil. The samples, 385-P4a, 385-143, and 385-179, were collected by Anthony Mariano. Samples 385-179 and 385-143 contain lamellar-twinned perovskite embayed and veined by anatase, whereas 385-P4a is composed primarily of anatase, exsolved magnetite, and only minor residual perovskite.

Samples were examined with a Philips 420 ST transmission electron microscope (TEM) operated at 120 keV. Samples were prepared by dispersing crushed grains on a holey carbon grid and by Ar-ion milling specimens removed from petrographic thin sections. Minerals were identified by their selected-area electron diffraction (SAED) patterns and by their compositions. Analytical electron microscope (AEM) data were obtained from the thin edges of samples using an EDAX Li-drifted Si de-

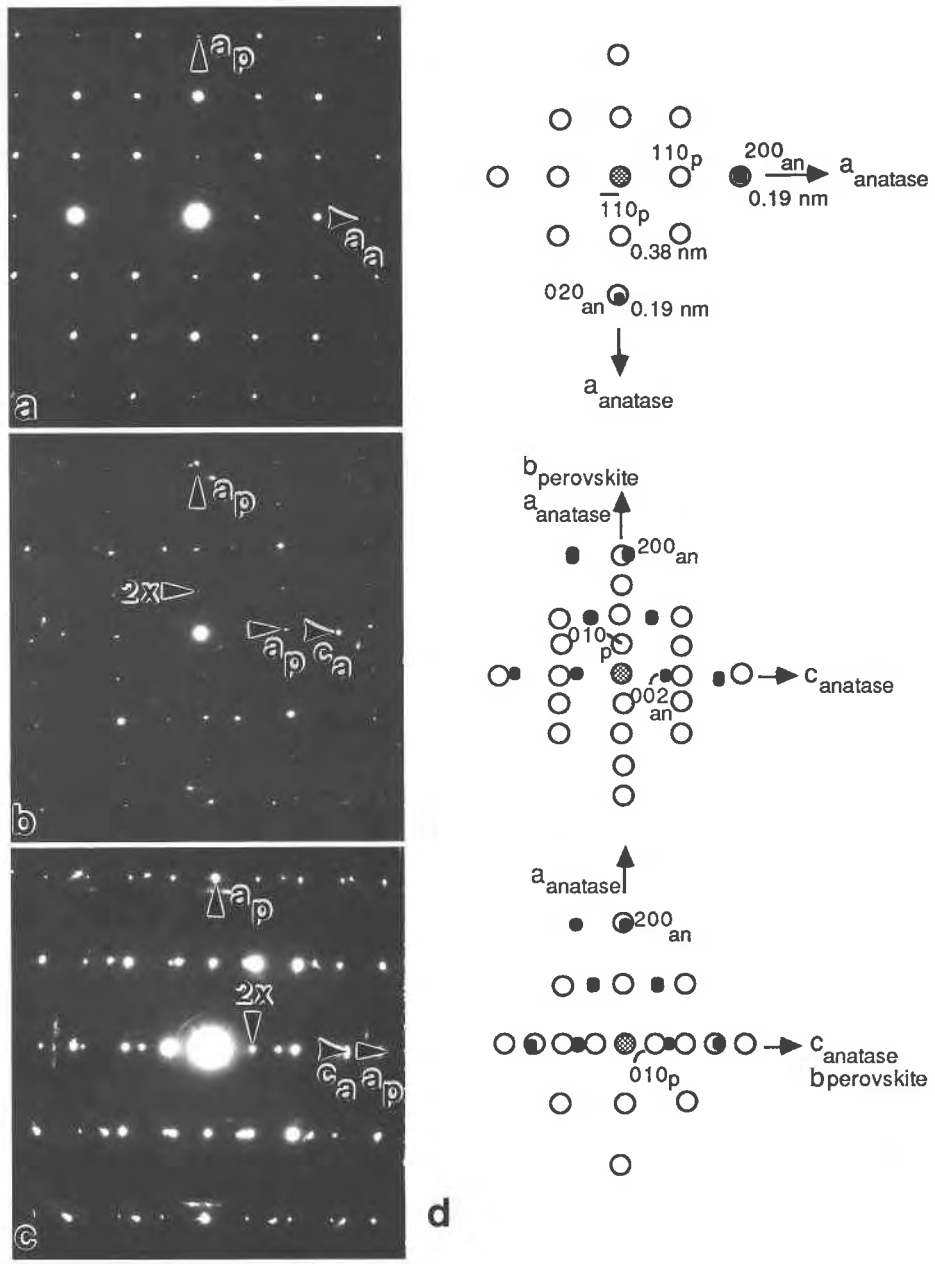

Fig. 9. SAED patterns (**a**) down [001] of anatase (a) and [001] of perovskite (p; pseudocubic unit cell); (**b**), (**c**) down [010] of anatase and [001] of perovskite. In the SAED pattern in **b** the [001] direction of anatase is perpendicular to and in **c** parallel to the doubled axis (2x) of perovskite (*b* of the orthorhombic cell). (**d**) Indexing of **a**, **b**, **c** using orthorhombic perovskite cell.

tector and processed with a Princeton Gamma-Tech System IV X-ray analyzer.

Anatase powder X-ray diffraction patterns were obtained using a Scintag automated powder diffractometer with Cu$K\alpha_1$ radiation. Peak positions were corrected for instrumental and physical aberrations through the use of internal standard lines from Si (Standard Reference Material 640b). Cell dimensions were determined using Latcon, a Scintag least-squares lattice parameter refinement program.

Experimental results

SAED patterns indicate that perovskite is largely replaced by anatase and that the reciprocal lattices of the minerals are oriented preferentially with respect to each other. When viewed with the beam parallel to [001] of anatase, it is apparent that the **a** axes of anatase are parallel and approximately equal in length to the pseudocubic **a** axes of perovskite (Fig. 9a). We make reference to the pseudocubic axes of perovskite because this setting

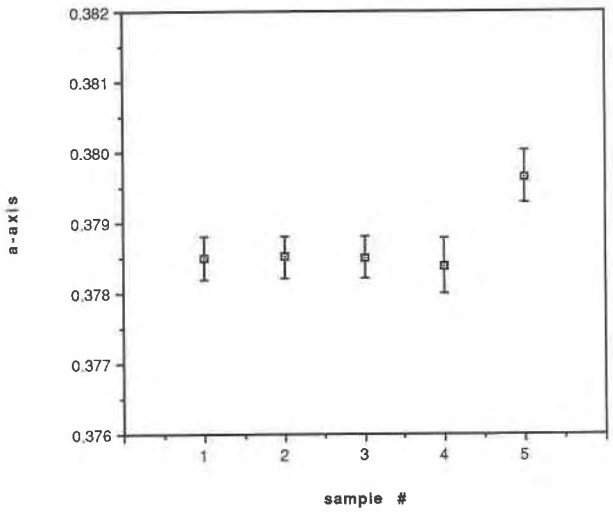

Fig. 10. Comparison between the lengths of the *a* axes (in nm) of undoped anatase: 1 = Cromer and Herrington (1955); 2 = JCPDS value; 3, 4 = values for undoped synthetic anatase determined using the procedures and equipment described here (Bischoff, in preparation) and for anatase replacing perovskite, 5. The 3σ error bars for the standard deviations from the refined *a*-axis dimensions are shown.

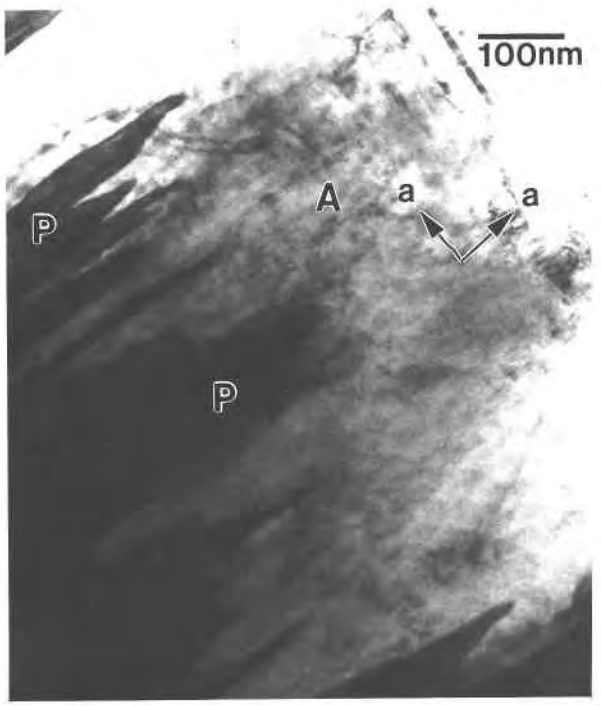

Fig. 11. Low-magnification electron micrograph down [001] of both anatase (A) and perovskite (P) showing little evidence for substantial volume change associated with the perovskite-anatase reaction.

permits an easier comparison with anatase. The relationship between the pseudocubic and orthorhombic cells is given by Megaw (1973) and White et al. (1985). For clarification, we have shown the orientation of the pseudocubic axes on the SAED patterns in Figures 9a, 9b, 9c and included the orthorhombic indices on the diagrams in Figure 9d. Although electron diffraction patterns show doubling of one axis (*b* of the orthorhomic perovskite structure), the **c** axis of anatase shows no tendency to preferential development parallel or perpendicular to this direction (Figs. 9b, 9c). Thus, as far as the weathering reactions are concerned, perovskite behaves as if it were cubic or pseudocubic. The origin of broad streaks and extra reflections in SAED patterns and the associated moiré fringes in images will be discussed below.

Areas clearly showing the contact between anatase and perovskite were rare. In general, either unaltered perovskite or porous aggregates of anatase were encountered. Where contacts were viewed with the beam parallel to [010] of anatase and to a pseudocubic **a** axis of perovskite, strips of anatase only a few tens of nanometers wide were preserved adjacent to the interface. No areas of amorphous Ti oxide were detected along the boundaries.

AEM analyses of the anatase typically showed the presence of 2–5% FeO (occasionally up to 10% FeO associated with goethite-anatase intergrowths), 1–2% CaO, and $<1\%$ Al_2O_3 and MgO. No other impurities were detected (e.g., Nb, REE). Figure 10 illustrates that the *a* axes of anatase after perovskite are demonstrably larger than values for pure anatase. The value determined for the *c* axis was smaller at the 1σ level but not significantly different at the 2σ level. The larger *a* dimension compared with undoped anatase may indicate cationic substitutions involving Fe^{3+}, OH, and interstitial Ca within the anatase.

At low magnification with the beam parallel to [001] of anatase (Fig. 11), anatase and perovskite were intimately intergrown and the material exhibited very low porosity. At higher magnification (Fig. 12), most interfaces between perovskite and anatase were approximately

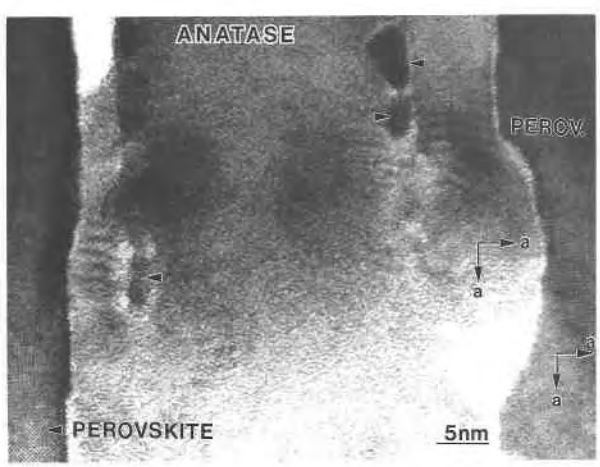

Fig. 12. High-resolution image down [001] of both anatase and perovskite showing the orientation of the interface between these minerals. Darker areas within the anatase (arrowed) may be relict strips of perovskite.

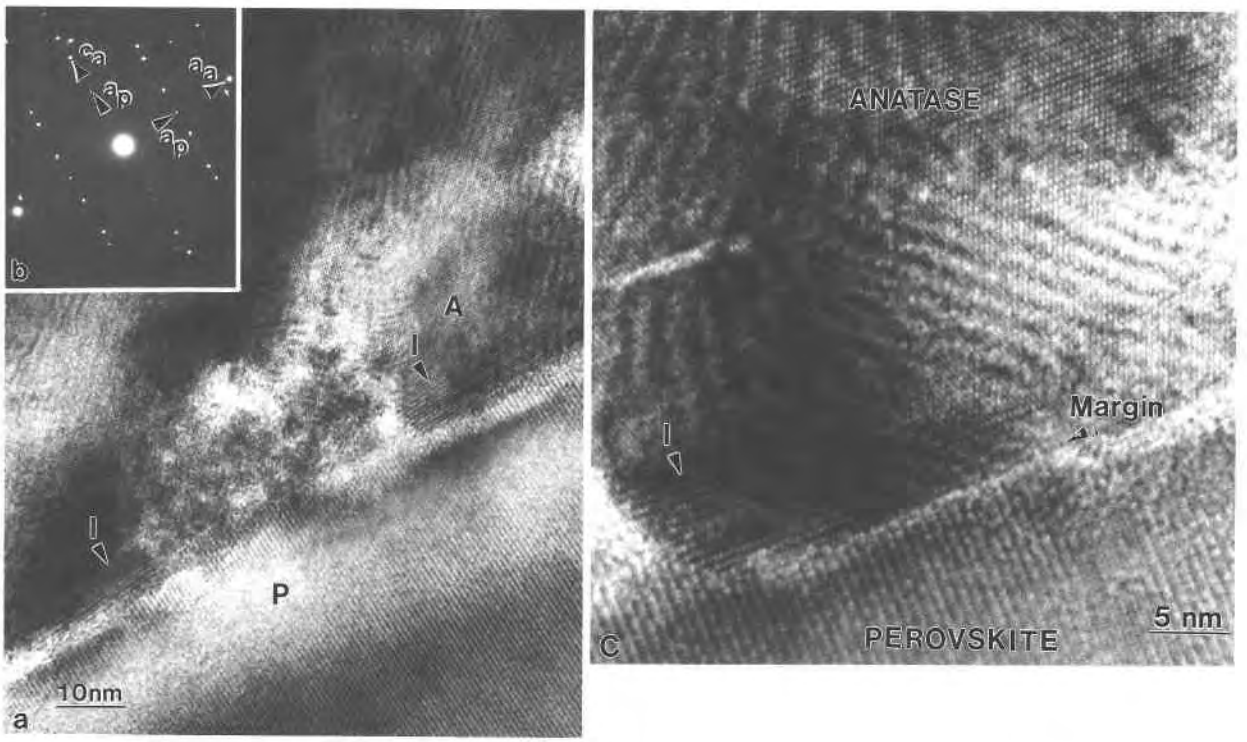

Fig. 13. (**a**) High-resolution image down [010] of anatase (A) and [001] of perovskite (P) showing the orientation of the interface. Strips of a third phase with a lattice spacing larger than those found in anatase are indicated (I). (**b**) SAED pattern. (**c**) Enlargement of the image in **a** showing the perovskite margin.

parallel to the pseudocubic **a** axes of perovskite and **a** axes of anatase. Lattice fringes are not present in the image of anatase because the spacings are so small that they were excluded by the objective aperture (spacings smaller than 0.22 nm were excluded). Lattice fringes associated with the irregular strips within anatase are probably associated with relict perovskite.

Figure 13 illustrates a contact between perovskite and anatase viewed down [010] of anatase. The numerous moiré fringes inclined (two orientations) to the interface are a sample preparation artefact (discussed below) and should be ignored. In addition to these, there is a set of fringes with a spacing of approximately 0.67 nm parallel to the interface and (001) of anatase. The spacing of these fringes cannot be readily explained as a moiré effect from overlapping perovskite and anatase, and they appear to be developed in areas where perovskite is clearly not present (Fig. 13c). These fringes were not observed at all contacts and are not present along interfaces other than those subparallel to (001) of anatase. The zone between the perovskite and all crystalline products is very narrow, generally <1 nm wide. No amorphous Ti oxide was detected in this region.

In addition to anatase, a second TiO_2 mineral was identified in these samples. SAED patterns indicated that this is TiO_2 (B) (Marchand et al., 1980), which has been reported by Banfield et al. (1991). TiO_2 (B) was present (in both ion-milled and crushed grain-mount samples) as homogeneous areas adjacent to perovskite surfaces (Fig. 14) and intergrown with anatase.

SAED patterns from the coexisting minerals indicated that the [011] TiO_2 (B) and [112] perovskite zones (pseudocubic axes) were subparallel, and (200) of TiO_2 (B) and $(\bar{1}10)$ of perovskite (pseudocubic axes) were inclined to each other by about 20°. The interface is subparallel to $(\bar{1}10)$ of perovskite (pseudocubic axes) and inclined to **c*** of TiO_2 (B) by about 45°.

When regions composed entirely of anatase were viewed down ⟨100⟩, the crystals were found almost always to contain planar gaps parallel to (001). These gaps give rise to streaking in some electron diffraction patterns (Fig. 15b).

The SAED patterns (Fig. 9) indicate that the **c** axis of anatase develops parallel to the three pseudocubic perovskite axes. Consequently, the weathered perovskite should contain crystals of anatase in three orientations. However, it is difficult to establish (statistically) whether **c** anatase develops parallel to each of these axes with equal probability.

Figure 16 illustrates an area composed of intergrown anatase crystals in both [001] and [100] orientations. The SAED pattern (Fig. 16b) indicates a very slight misorientation between the (001) and (100) planes of the two sets of crystals.

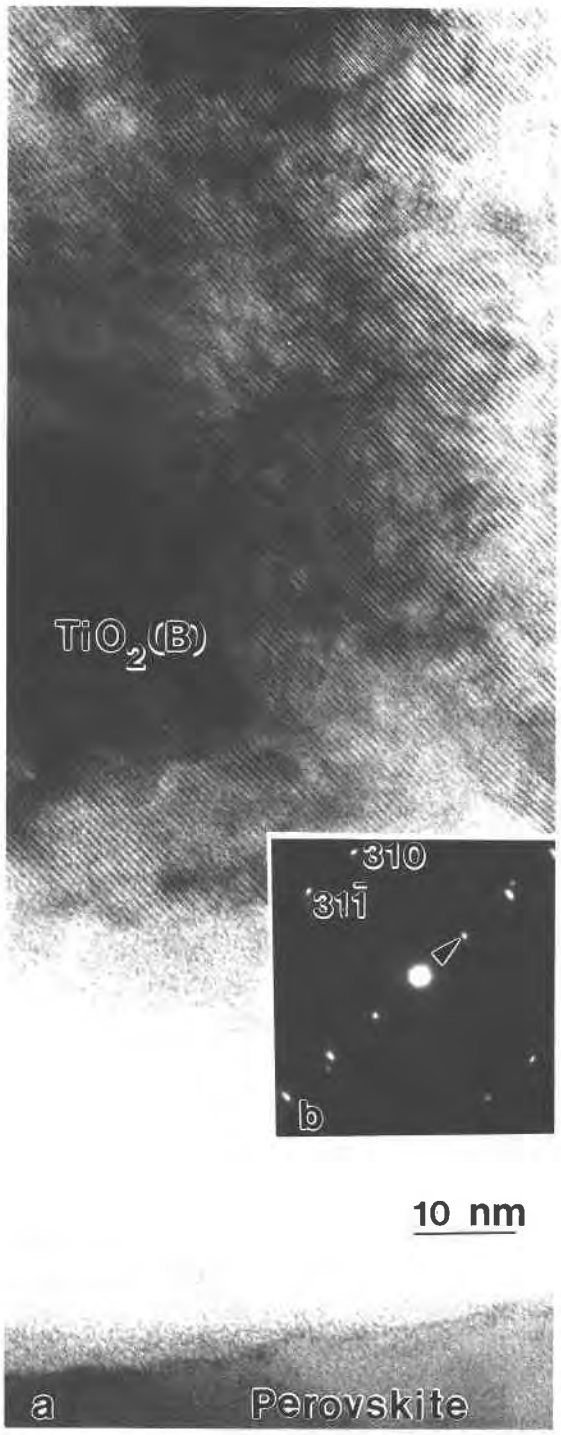

Fig. 14. (**a**) Image showing an area of TiO_2 (B) exhibiting 0.62-nm (001) fringes. TiO_2 (B) adjacent to perovskite has been destroyed by ion milling. (**b**) SAED pattern from TiO_2 (B). Arrow indicates the **c*** direction.

Although some areas of anatase viewed with the beam parallel to [001] show little porosity, some aggregates of needle-shaped anatase crystals with a high intercrystal porosity were occasionally noted (Fig. 17). The interiors

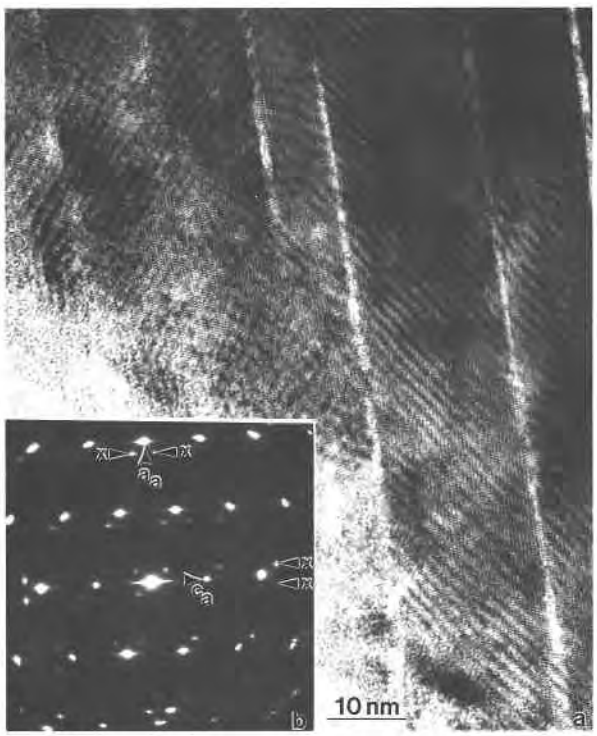

Fig. 15. (**a**) High-resolution image down [010] of anatase showing regular gaps parallel to the (002) fringes. Moiré fringes are inclined to (002) fringes. (**b**) SAED pattern. X indicates additional reflections referred to in the text.

of crystals show signs of recrystallization and elimination of very fine-scale porosity.

The anatase is extensively intergrown with Ca-bearing light rare earth element (LREE) phosphate minerals (Fig. 18). Previous work (Mariano, 1989) has shown that the

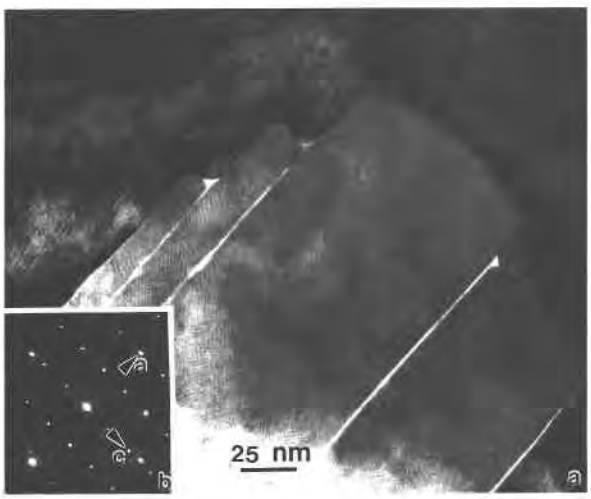

Fig. 16. (**a**) Low-magnification image showing an intergrowth of anatase crystals oriented with their [001] directions both perpendicular (as indexed) and parallel to the beam. (**b**) SAED pattern from area shown in **a**.

Fig. 17. Aggregate of anatase needles with a high intercrystal porosity.

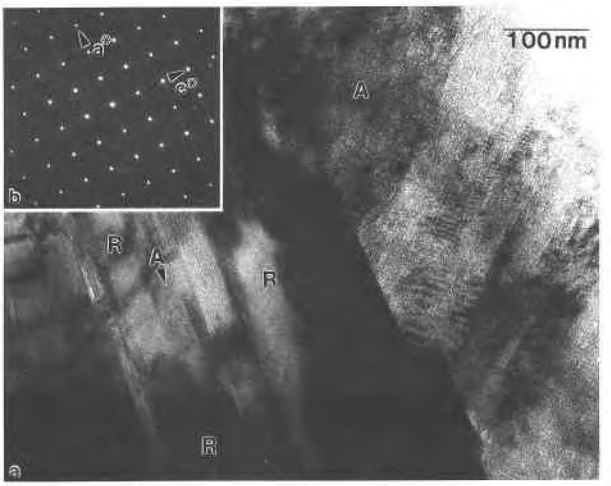

Fig. 18. (**a**) Low-magnification image showing intimately intergrown anatase (A) and rhabdophane (R). (**b**) SAED pattern from rhabdophane.

LREE pattern of the minerals is identical to that of the perovskite, indicating that the REEs were released from the perovskite and reprecipitated without fractionation. SAED patterns from several zone axes were recorded from needles such as those shown in Figure 18. These SAED patterns were consistent with the identification of this mineral as rhabdophane. Sample 385-P4a also contains abundant, complexly exsolved magnetite that shows no sign of alteration.

Sample preparation artefacts

Most of the specimens examined in this study were prepared for transmission electron microscopy by Ar-ion milling without liquid N_2 cooling of the specimen. All diffraction patterns from the anatase samples prepared in this way showed extra reflections (particularly apparent in Figs. 9c, 13b, 15b) that could be indexed to a cubic unit cell with $d_{200} = 0.21$ nm that developed in two orientations with the ⟨100⟩ directions slightly rotated to either side of the tetragonal anatase axes. Moiré fringes in high-resolution images (Figs. 13a, 15a) were pervasive, occurring in small patches in two symmetry-related orientations over the entire sample. Dark-field images suggest that the phase causing the moirés was more abundant along the sample margins. Diffraction patterns and images from crushed grains of anatase samples showed no evidence of extra spots or moiré fringes. Furthermore, specimens prepared by ion milling using a liquid-N_2-cooled stage did not show the extra reflections or moiré fringes. We conclude that a surface-coating phase formed during non-cooled ion milling. Based on the size and shape of the unit cell, we tentatively suggest that the material is a surface coating of TiO. In any case, the extra spots and moiré fringes should be ignored since they are not related to the natural sample microstructure.

Discussion

Perovskite alteration

Perovskite is a major igneous mineral in the Salitre II carbonatite. Some altered samples are almost completely composed of TiO_2 minerals that pseudomorph the perovskite. The coexistence of anatase and TiO_2 (B) with rhabdophane, calcite, and goethite supports the currently held view (Mariano, 1989) that the replacement of perovskite by Ti minerals occurred as the result of weathering.

SAED patterns and images from intergrown perovskite, anatase, and TiO_2 (B) (Figs. 9, 13) clearly demonstrate that the TiO_2 minerals replacing perovskite are topotactically oriented. The anatase intergrowths composed of crystals in two or more orientations (Fig. 16) may reflect initiation of the anatase-forming reaction at separate sites in the perovskite. The direct overgrowth of TiO_2 minerals in specific orientations onto the perovskite surface is consistent with the possibility that the reactions involve direct structural inheritance of parts of the Ti-O framework of perovskite.

Alternative mechanisms, (1) dissolution followed by reprecipitation or (2) dissolution followed by formation of an amorphous Ti intermediate and crystallization of anatase, are not inconsistent with the topotactic relationship described above. However, given the extremely low solubility of Ti under weathering conditions, a mechanism involving complete congruent dissolution of perovskite seems unlikely. Furthermore, Jostsons et al. (1990) report no Ti in the solutions associated with hydrothermal perovskite dissolution experiments. The perovskite-TiO_2 mechanism suggested by Kastrissios et al. (1986, 1987) and Myhra et al. (1984) emphasizes the importance of Ca leaching and development of a disordered or amorphous Ti-rich surface layer. Because we find no evidence for an amorphous Ti phase along the interface between

anatase and perovskite (e.g., Fig. 13), we suggest that this mechanism does not predominate during surficial weathering.

High-resolution images indicate that the interface region between perovskite and anatase is very narrow (<1 nm wide; Fig. 13c). If this remaining perovskite is to be converted to anatase without large-scale solution transport of Ti, Ca leaching and structural reorganization must occur along this planar region. In a zone as narrow as this, distinguishing among transport of components through a solution layer, surface restructuring, growth of an amorphous intermediate film, and direct structural inheritance is extremely difficult.

The presence of two metastable polymorphs in place of the thermodynamically stable polymorph rutile suggests the importance of kinetic and structural factors in determining the reaction products. The formation of these polymorphs may be controlled by the specific structural inheritance involved in the reaction mechanisms or by the structure of the surface onto which epitactic growth occurs.

The growth of two TiO_2 minerals suggests that decalcification of perovskite can occur by alternate routes with similar energetic requirements. Although anatase is by far the predominant Ti-bearing alteration product, the presence of TiO_2 (B) is of significance. TiO_2 (B) has been reported in low-grade metamorphic rocks (Banfield et al., 1991), but it has not been recognized previously as a weathering product.

Images recorded with the beam parallel to [001] of anatase (e.g., Fig. 11) suggested that the areas occupied by reactant and product structures is approximately the same, as observed in this orientation. Contacts between perovskite and anatase showing the third dimension of the intergrowths (beam parallel to ⟨100⟩ anatase) and preserving strips of anatase greater than a few nanometers wide were extremely rare. In regions where perovskite had been completely destroyed, the anatase contained abundant gaps (Fig. 15), suggesting that a substantial reduction in volume occurs parallel to [001] of anatase.

Recrystallization of the anatase to form arrays of elongate crystals results in the appearance of very large holes. The very significant volume change associated with the perovskite-anatase reaction is particularly apparent where this recrystallization has occurred.

The perovskite to anatase and TiO_2 (B) reactions

It is not possible to use textural arguments to prove that transformations involved leaching of Ca and reconstruction of the existing Ti-O framework rather than occurring through a transient amorphous intermediate. We favor the former mechanism because (1) an amorphous phase was not detected and (2) the direct mechanisms described below, which are a consequence of the close structural relationships between perovskite, anatase, and TiO_2 (B), provide reasonable reaction pathways consistent with the orientation relationships between reactant and products.

Figure 19a shows an idealized (undistorted) representation of the perovskite structure viewed down ⟨100⟩ (pseudocubic axes). Orthorhombic distortions from this idealized cubic arrangement involve displacement of the O atoms with minimal disruption of the cation array (O'Keefe and Hyde, 1977; White et al., 1985).

The conversion of perovskite to anatase and TiO_2 (B) requires elimination of Ca, which is transported away from the reaction site and reprecipitated as calcite in other areas. The reaction also requires conversion of some corner-linked to edge-linked pairs of octahedra. The removal of every second plane of Ca atoms by leaching and the collapse of the Ti-O framework, as indicated by the arrows in Figure 19a, generate a hypothetical structure (Figs. 19b, 19c) with the composition $Ca_{0.5}TiO_{2.5}$. This structure is closely related to sheared perovskite derivative structures in the $(Na,K,Ca,Nb)TiO_x$ system (Hyde and Andersson, 1988). The arrangement of more darkly stippled octahedra in Figures 19b and 19c is found in the TiO_2 (B) structure.

The micrographs shown in Figures 13a and 13c illustrate a phase developed at the interface between anatase and perovskite that is characterized by a 0.67-nm spacing perpendicular to the interface, between that of d_{200} of anatase (0.475 nm) and the 0.77-nm spacing equivalent to [020] perovskite (pseudocubic axes). Because this material has the characteristics predicted for the intermediate, partly decalcified weathering product (Figs. 19b, 19c), it may have the structure shown in Figure 19c.

The second step to form anatase from the intermediate phase may occur by removal of the remaining Ca and collapse of the Ti-O framework, as indicated by the arrows in Figure 19c. The experimentally observed orientations of the intergrown perovskite and anatase, the presence of what is interpreted to be the predicted intermediate phase, the orientations of the interfaces between the three phases, the seemingly small volume change associated with the intergrowths in two dimensions, and the significant volume change associated with the third dimension parallel to [001] of anatase are all consistent with the view that perovskite is converted to anatase by leaching and structural collapse as illustrated in Figure 19. Consequently, the reaction can be written $2CaTiO_{3(perov.)} \rightarrow 2Ca_{0.5}TiO_{2.5(int.)} + Ca^{2+}_{(aq)} + O^{2-}_{(aq)} \rightarrow 2TiO_{2\,(anatase)} + 2Ca^{2+}_{(aq)} + 2O^{2-}_{(aq)}$. The actual aqueous species are not known.

The TiO_2 (B) structure can be generated from the intermediate, partly decalcified structure (Fig. 19c) by an alternative second step that involves Ca removal and collapse of the Ti-O framework as indicated in Figures 19e and 19f. This reaction can be written $2CaTiO_{3\ (perov.)} \rightarrow 2Ca_{0.5}TiO_{2.5\ (int.)} + Ca^{2+}_{(aq)} + O^{2-}_{(aq)} \rightarrow 2TiO_{2\ (B)} + 2Ca^{2+}_{(aq)} + 2O^{2-}_{(aq)}$. Consequently, we suggest that the formation of TiO_2 minerals from perovskite during weathering can be attributed to stepwise decalcification, with alternative directions of second-stage collapse of the Ti-O framework resulting in either anatase of TiO_2 (B). The conversion of perovskite to TiO_2 minerals by a mechanism involving

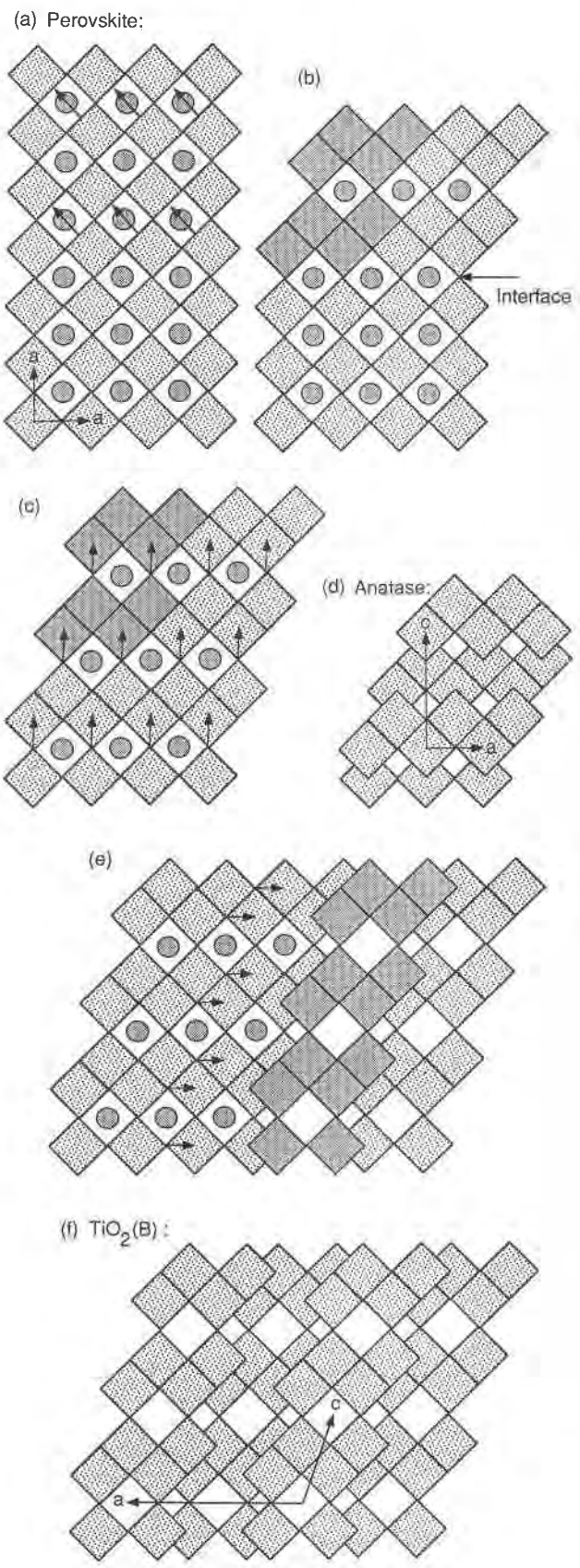

structural collapse eliminates the requirement for large-scale transport of Ti in solution.

For the reaction to involve inheritance of slabs of the perovskite Ti-O framework, it is necessary to remove Ca. The presence of abundant gaps perpendicular to the directions of volume reduction and the proposed structural collapse suggest that relatively narrow slabs of perovskite react at one time. A possible mechanism involves leaching of Ca from the surface layer (as occurs to depths of at least 3 nm in labradorite dissolution; Hochella et al., 1988), with charge balance maintained by bonding of two H^+ to two O atoms. This leaching opens pathways (via the vacant Ca sites) to the interior of the crystal, through which Ca could be transported to the surface. Collapse as indicated by Figure 19a superimposes the two OH groups, so that the excess structural O can be eliminated as H_2O. This could be written $CaTiO_3 + 2H^+ \rightarrow Ca^{2+} + H_2TiO_3$; $H_2TiO_3 \rightarrow TiO_2 + H_2O$.

In this study we have not detected amorphous Ti oxide or brookite in the alteration assemblage, which distinguishes the weathering reaction from the reaction studied experimentally at higher temperatures (e.g., Kastrissios et al., 1987). The absence of brookite is not surprising if, as we suggest, the natural weathering reactions involve a direct structural transformation. As shown in Figure 4, the brookite structure contains anatase-type slabs in a second orientation that cannot be generated from the perovskite or intermediate structure by simple collapse of the Ti-O framework.

Conclusions

We have presented a way of viewing the TiO_2 structures that highlights their similarities and provides clues to the mechanisms by which the polymorphic transformations between them occur. Considering these structures to be constructed from slabs or blocks related by shear or cation displacement simplifies the study of the perovskite to anatase and TiO_2 (B) weathering reactions (this study) and the TiO_2 (B) to anatase (Brohan et al., 1982; Banfield et al., 1991) and rutile–TiO_2 II transformation mechanisms (Hyde and Andersson, 1988).

The FBB approach to interpreting other transformation mechanisms, such as brookite or anatase to rutile or TiO_2 (H) to anatase, cannot yet be assessed. However, we have made predictions about these reactions that can be tested with future experimental work. If an FBB description appropriate to all the observed transformations could be found, it would further enhance understanding of the relationships between these minerals.

The results of the perovskite weathering study suggest that the reactions involve direct structural inheritance of planes of corner-linked Ti octahedra and proceed by step-

←

Fig. 19. Diagram illustrating the stepwise conversion of perovskite (viewed down one pseudocubic axis) to anatase (**a**), (**b**), (**c**), (**d**); and TiO_2 (B) (**a**), (**b**), (**e**), (**f**).

wise removal of Ca and structural collapse to form edge-sharing octahedral pairs. Although some redistribution of Ti by dissolution and reprecipitation may occur (e.g., during recrystallization), the mechanism described here eliminates the need for large-scale solution transport of this very insoluble element. The formation of anatase and TiO_2 (B), rather than other TiO_2 polymorphs, emphasizes the importance of the structure of the precursor mineral in determining the weathering product formed.

Acknowledgments

We thank Anthony Mariano for providing the weathered Salitre II carbonatite samples and initial information about their mineralogy. Timothy White, George Guthrie, Jeffrey Post, and Dimitri Sverjensky provided helpful comments that greatly improved this manuscript. This work was supported by NSF grant EAR-8903630.

References cited

Andersson, S. (1969) Mechanism of transformation of rutile → α-PbO_2. A simple cation rearrangement. Bulletin de la Societé Chimique de France, 4, 1065–1066.

Banfield, J.F., Veblen, D.R., and Smith, D.J. (1991) The identification of naturally occurring TiO_2 (B) by structure determination using high-resolution electron microscopy, image simulation, and distance-least-squares refinement. American Mineralogist, 76, 343–353.

Baur, W.H. (1961) Atomabstände und bindungswinkel im brookit, TiO_2. Acta Crystallographica, 14, 214–216.

Brohan, L., Verbaere, A., and Tournoux, M. (1982) La transformation TiO_2 (B) → anatase. Materials Research Bulletin, 17, 355–361.

Bursill, L.A. (1979) Structural relationships between β-gallia, rutile, hollandite, psilomelane, ramsdellite and gallium titanite type structures. Acta Crystallographica, B35, 530–538.

Bursill, L.A., and Hyde, B.G. (1972) Rotation faults in crystals. Nature—Physical Science, 240, 122.

Coe, R.S., and Kirby, S.H. (1975) The orthoenstatite to clinoenstatite transformation by shearing and reversal by annealing: Mechanism and potential applications. Contributions to Mineralogy and Petrology, 52, 29–55.

Cromer, D.T., and Herrington, K. (1955) The structures of anatase and rutile. Journal of the American Chemical Society, 77, 4708–4709.

Dachille, F., Simons, P.Y., and Roy, R. (1968) Pressure-temperature studies of anatase, brookite, rutile, and TiO_2 (II). American Mineralogist, 53, 1929–1939.

Hochella, M.F., Ponader, H.B., Turner, A.M., and Harris, D.W. (1988) The complexity of mineral dissolution as viewed by high resolution scanning Auger microscopy: Labradorite under hydrothermal conditions. Geochimica et Cosmochimica Acta, 52, 385–394.

Hyde, B.G. (1987) The effect of non-bonded, anion-anion interactions on the $CaCl_2$/rutile transformation and on the bond lengths in the rutile type. Zeitschrift für Kristallographie, 179, 205–213.

Hyde, B.G., and Andersson, S. (1988) Inorganic crystal structures, 430 p. Wiley Interscience, New York.

Hyde, B.G., and O'Keefe, M. (1973) Relations between the DO_9 (ReO_3) structure type and some 'bronze' and 'tunnel' structures. Acta Crystallographica, A29, 243–248.

Hyde, B.G., Bagshaw, A.N., O'Keefe, M., and Andersson, S. (1974) Defect structures in crystalline solids. Annual Review of Material Science, 4, 43–92.

Jostsons, A., Smith, K.L., Blackford, M.G., Hart, K.P., Lumpkin, G.R., McGlinn, P., Myhra, S., Netting, A., Pham, D.K., Smart, R.St.C., and Turner, P.S. (1990) Description of Synroc durability: Kinetics and mechanisms of reaction. NERDDP Report no. 1319, 261 p. ANSTO Lucas Heights Research Laboratories, New South Wales, Australia.

Kang, Z., and Bao, Q.X. (1986) A study of the interaction of V_2O_5/TiO_2 (anatase) by high-resolution electron-microscopy (HREM). Applied Catalysis, 26, 251–263.

Kastrissios, T.K., Stephenson, M., Turner, P.S., and White, T.J. (1986) Epitaxial growth of TiO_2 polymorphs on perovskite. Proceedings of the 11th International Congress on Electron Microscopy, Kyoto, 1697–1698.

Kastrissios, T.K., Stephenson, M., and Turner, P.S. (1987) Hydrothermal dissolution of perovskite: Implications for Synroc formulation. Journal of the American Ceramic Society, 70, C144–C146.

Kay, H.F., and Bailey, P.C. (1957) Structure and properties of $CaTiO_3$. Acta Crystallographica, 10, 219–226.

Latroche, M., Brohan, L., Marchand, R., and Tournoux, M. (1989) New hollandite oxides; TiO_2 (H) and $K_{0.06}TiO_2$. Journal of Solid State Chemistry, 81, 78–82.

Marchand, R., Brohan, L., and Tournoux, M. (1980) TiO_2 (B), a new form of titanium dioxide and the potassium octatitanate $K_2Ti_8O_{17}$. Materials Research Bulletin, 15, 1129–1133.

Mariano, A.N. (1989) Economic geology of rare earth elements. In Mineralogical Society of America Reviews in Mineralogy, 21, 309–337.

Megaw, H.D. (1973) Crystal structures: A working approach, 563 p. W.B. Saunders, Philadelphia.

Moore, P.B. (1986) Quartz: Variations on a theme. American Mineralogist, 71, 540–546.

Myhra, S., Savage, D., Atkinson, A., and Riviere, J.C. (1984) Surface modification of some titanate minerals subjected to hydrothermal chemical attack. American Mineralogist, 69, 902–909.

Navrotsky, A., and Kleppa, O.J. (1967) Enthalpy of the anatase-rutile transformation. Journal of the American Ceramic Society, 50, 626.

Nesbitt, H.W., Bancroft, G.M., Fyfe, W.S., Karkhanis, S.N., and Nishijima, A. (1981) Thermodynamic stability and kinetics of perovskite dissolution. Nature, 289, 358–362.

O'Keefe, M., and Hyde, B.G. (1977) Some structures topologically related to cubic perovskite ($E2_1$), ReO_3 (DO_9) and Cu_3Au ($L1_2$). Acta Crystallographica, B33, 3802–3813.

Post, J.E., and Burnham, C.W. (1986) Ionic modeling of mineral structures and energies in the electron gas approximation: TiO_2 polymorphs, quartz, forsterite, and diopside. American Mineralogist, 71, 142–150.

Shannon, R.D., and Pask, J.A. (1964) Topotaxy in the anatase-rutile transformation. American Mineralogist, 49, 1707–1717.

Simons, P.Y., and Dachille, F. (1967) The structure of TiO_2-II, a high pressure phase of TiO_2. Acta Crystallographica, 23, 334–335.

——— (1970) Possible topotaxy in the TiO_2 system. American Mineralogist, 55, 403–415.

Tournoux, M., Marchand, R., and Brohan, L. (1986) Layered $K_2Ti_4O_9$ and the open metastable TiO_2 (B) structure. Progress in Solid State Chemistry, 17, 33–52.

Veblen, D.R. (1991) Polysomatism and polysomatic series: A review and applications. American Mineralogist, 76, 801–826.

White, T.J., Segall, R.L., Barry, J.C., and Hutchison, J.L. (1985) Twin boundaries in perovskite. Acta Crystallographica, B41, 93–98.

Manuscript received April 22, 1991
Manuscript accepted December 18, 1991